When low-vision task meets dense prediction tasks with less data: an auxiliary self-trained geometry regularization

Anonymous authors
Paper under double-blind review

Abstract

Many deep learning methods are data-driven, often converging to local minima due to limited training data. This situation poses a challenge in domains where acquiring adequate data is difficult for model training or fine-tuning, such as generalized few-shot semantic segmentation (GFSSeg) and monocular depth estimation (MDE). To this end, we propose a self-trained geometry regularization framework to enhance model training or fine-tuning in scenarios with limited training data using geometric knowledge. Specifically, we propose to leverage low-level geometry information extracted from the training data and define a novel regularization term, which is a plug-and-play module jointly trained with the primary task via multi-task learning. Our proposed regularization neither relies on extra manual labels and data in training nor requires extra computation during the inference stage. We demonstrate the effectiveness of this regularization on GFSSeg and MDE tasks. Notably, it improves the state-of-the-art GFSSeg by 5.61% and 4.26% mIoU of novel classes on PASCAL and COCO in the 1-shot scenario. In MDE, it achieves a relative reduction of SILog error by 16.6% and 9.4% for two recent methods in the KITTI dataset.

1 Introduction

The recent advancements in deep learning-based approaches have been enormous and promising. Various modern and sophisticated deep neural networks (Dosovitskiy et al., 2020; Liu et al., 2021; Oquab et al., 2023; Carion et al., 2020; Touvron et al., 2022) have been proposed to address diverse tasks. These deep learning models are mostly data-driven and need much training data (Zhou et al., 2017; Deng et al., 2009; Russakovsky et al., 2015; Kuznetsova et al., 2020), avoiding suffering from local minimum convergence. Meanwhile, in practice, annotating a large number of training samples is exceedingly challenging, particularly for tasks involving dense predictions. For example, in monocular depth estimation (MDE), collecting large-scale data with paired ground truth is costly (Ranftl et al., 2022; Bhat et al., 2023; Ranftl et al., 2021a; Piccinelli et al., 2024). Additionally, in generalized few-shot semantic segmentation (GFSSeg) (Tian et al., 2022; Hajimiri et al., 2023; Liu et al., 2023a; Lang et al., 2022), only a few shots of data can be used to adapt the models to novel classes. Therefore, there remain many challenges in dense prediction tasks with less data.

One way to combat against this issue is to train the network for fundamental task-invariant features via self-supervised learning with a large scale of unlabelled data (Chen et al., 2020; Caron et al., 2021; Bao et al., 2022; He et al., 2022), which will be further fine-tuned for downstream tasks with much smaller task-specific annotated data. In (Darcet et al., 2023; Oquab et al., 2023), robust visual features are first learned without supervision, followed by evaluating two dense downstream tasks, semantic image segmentation and depth estimation. However, such approaches need carefully designed regularization modules to avoid representation collapse (Grill et al., 2020; Caron et al., 2021; He et al., 2020; Oquab et al., 2023) and may also suffer from catastrophic forgetting in model fine-tuning (Li et al., 2023b; Xu et al., 2023b).

Another idea is to employ geometry regularization. Encoding geometry constraints via auxiliary learning helps the model to learn the task-invariant features, benefiting the convergence of the primary task. Edge or semantic information can be considered as examples of geometry information. Some earlier works (Ramirez et al., 2018; Fu et al., 2018b; Zhang et al., 2019a; Zhu et al., 2020) have shown that joint detection of edge

and semantic labels can improve performance in medical image analysis and depth estimation. Some other methods use edges or semantics to guide the main tasks (e.g., depth estimation) via iterative fine-tuning (Shao et al., 2023b; Xu et al., 2023a) or other post-processing (Su & Tao, 2023). While geometric regularization is usually effective, the difficulty lies in acquiring different geometry constraints. Semantic labels often provide more geometric information compared to edges, yet the acquisition is also more challenging.

This work proposes a new auxiliary plug-and-play geometry regularization network (GRNet) to improve model training. Unlike previous methods that fuse low-level features into the primary task with increased computation, GRNet is discardable and does not lead to additional computational costs at the inference stage. In addition, we propose a novel primary-to-auxiliary aggregation module in GRNet to consider the association between the primary task and the regularization task. Rethinking the usages of geometry constraints, we aim to introduce an accessible yet effective low-level geometry regularization. Unlike the previous methods that mainly use edges, we investigate different low-level geometry information while the edge is just a special case. Specifically, in the auxiliary regularisation term, we investigate keypoints, e.g., SuperPoint (DeTone et al., 2018), scare-invariant feature transform (SIFT) (Lowe, 2004), and edges, e.g., Canny edges (Canny, 1986), as pseudo ground truths. Our results show that both keypoints and edges work well to improve the results and that different choices of low-level geometries lead to similar improvement.

The keypoints work as keypoint regularization brings in additional subtasks similar to edge regularization. Based on recent progress in model-based deep learning (Shlezinger et al., 2020), additional regularization often help the model training and reduces over-fitting. The fact that keypoint work in segmentation validates and supports our hypothesis that the deep learning model trained from a small dataset can be biased. Previous researchers have used edge as a supervisor signal to improve segmentation (Yu et al., 2018) and depth estimation (Zhu et al., 2020). It is true that such information helps. However, our research shows that model bias is another major factor compromising performance. Including additional terms such as edge is a special case that would improve model generalization and, therefore, better performance. To validate and support our hypothesis, we used a key point it is not directly related to segmentation and showed that it also helps.

The benefits of the proposed auxiliary GRNet are three-fold. Firstly, it improves the feature extraction in the backbone to make it more effective for multiple tasks. Secondly, by integrating the output of the primary task into an auxiliary low-level structure detection task through a primary-to-auxiliary aggregation module, we can post a constraint on the output of the primary task. Surprisingly, different choices of geometry knowledge, such as edges and key points, improve the performance of the main tasks comparably. This helps us better understand the role of auxiliary edge detection in previous methods, which we will discuss in more detail in Section 4.1.4 and Section 4.2.3. Thirdly, it is easier to obtain low-level structures than semantic labels for regularization. For example, the edges can be estimated by pretrained deep learning models or traditional handcrafted methods such as the Canny edge detector (Canny, 1986). The key points can be easily computed by SIFT (Lowe, 2004) and self-supervised SuperPoint model (DeTone et al., 2018).

It shall be highlighted that our method is conceptually different from many existing methods (Li et al., 2020; Lu et al., 2022; Li et al., 2024). Our method uses the output $\mathbf{p}$ of the primary task as one of the inputs of the auxiliary task. Such a design encourages the network to compute $\mathbf{p}$ in favour of the auxiliary task, i.e., the network would compute $\mathbf{p}$ that leads to lower loss of the auxiliary task. This is equivalent to imposing a constraint on the output $\mathbf{p}$ such that it favours low-level geometry extraction in the auxiliary task. It differs from other methods that directly apply post-processing smoothing to the output. Moreover, this auxiliary geometry aggregation module would be discarded after the training, and it would not lead to any extra computational cost at the inference stage.

The major contributions of this paper are:

- We propose a simple yet effective self-trained geometry regularization, which uses the accessible low-level geometry information to construct a regularization term for training the dense prediction tasks via multi-task learning.
- We propose a primary-to-auxiliary geometry aggregation module to consider the association between the primary and auxiliary tasks. It encourages the primary branch to predict output in favour of the auxiliary task, which differs from post-processing fusion or smoothing in previous methods.

- We integrate the proposed regularization term with different approaches on GFSSeg and MDE tasks. Experimental results show that it is generic for different architectures and tasks.

2 Related works

2.1 Dense Prediction Tasks with Less Data

Dense prediction tasks refer to tasks where prediction for each pixel is needed, such as depth estimation (Laina et al., 2016; Yuan et al., 2022; Patil et al., 2022; Shao et al., 2023a; Yang et al., 2024; Ranftl et al., 2020; Bhat et al., 2023; Li et al., 2023a; Kirillov et al., 2023), semantic image segmentation (Zhao et al., 2017; Chen et al., 2017; Cheng et al., 2022; Xie et al., 2021; Li et al., 2023a; Isensee et al., 2021), etc. Recently, The Segment Anything model and Depth Anything model have shown that large-scale data is important in improving the performance of dense prediction tasks (Ranftl et al., 2021b; Kirillov et al., 2023; Bhat et al., 2023; Yang et al., 2024). However, obtaining large-scale data in some tasks is challenging. For example, around 63 million images are collected for training the Depth Anything model (Yang et al., 2024), and 12 million for the Segment Anything model (Kirillov et al., 2023). It is more difficult to train with large-scale data. Without pursuing training with large-scale data, we aim to design accessible yet effective geometry regularization for dense prediction tasks with less data. In this paper, we use generalized few-shot semantic segmentation (GFSSeg) and monocular depth estimation (MDE) as two examples to validate our approach, where both tasks face data scarcity issues.

In the GFSSeg (Tian et al., 2022), we need to adapt the models to novel classes while maintaining their performances in base classes using only a few shots of data with novel class. Tian et al. (2022) proposed context-aware prototype learning (CAPL), which mines contextual cues from support and query samples to enrich the classifier for the novel class segmentation. Liu et al. (2023a) proposed to leverage projection onto orthogonal prototypes (POP) to generalize well on base classes and quickly adapt to new objects or instances. We use these two methods as baselines to evaluate the effectiveness of our method in GFSSeg. Hajimiri et al. (2023) propose leveraging the InfoMax principle to maximize Mutual Information (MI) between learned feature representations and predictions with an easily optimized inference phase.

In MDE, some approaches (Ranftl et al., 2020; Bhat et al., 2023; Yang et al., 2024; Piccinelli et al., 2024) endeavour to gather as much data as possible to train a robust model. Ranftl et al. (2020) try to mix multiple datasets from different sources and propose a robust training objective to boost the depth estimation performance. Bhat et al. (2023) propose the first approach that combines both worlds, leading to a model with excellent generalization performance in MED while maintaining metric scale. Built upon (Bhat et al., 2023), Yang et al. (2024) extend the training image scale to 63 million, achieving impressive generalization ability. Such large-scale training data poses significant challenges for both data collection and model training processes. Recent other works (Shao et al., 2023b; Yuan et al., 2022; Shao et al., 2023a) popularly employ the vision transformer. Leveraging the pretrained transformer (Liu et al., 2021) as a backbone encoder, Yuan et al. (2022) proposed neural window fully-connected conditional random fields (NeWCRFs) as depth decoder, showing promising performance in MDE task. Based on NeWCRFs, a physics-regularization is proposed to consider a normal distance map in the depth estimation (Shao et al., 2023a). Shao et al. (2023b) proposed Iterative elastic Bins (IEbBins), which modifies the regression task to the classification task and adopts an iterative post-processing to improve the results. However, it requires 129% extra computational cost.

In this work, we use NeWCRFs as our baseline, and we find that our GRNet can improve the NeWCRFs by 7.4% and 16.6% in NYUv2 (Nathan Silberman & Fergus, 2012) and KITTI (Geiger et al., 2013). Compared with IEbBins, GRNet with NeWCRFs can achieve comparable or better performance without using its iterative post-processing and, therefore, avoids the 129% extra computational cost.

2.2 Auxiliary Edge and Semantic Detection

Previously, many methods have been proposed to use edge detection or semantic segmentation to improve the performance of main tasks. Ramirez et al. (2018) proposed to leverage the semantics and geometry by enforcing spatial proximity between depth discontinuities and semantics for monocular depth estimation.

Wu et al. (2019) proposed pyramid cost volumes to capture semantic and multi-scale spatial information for semantic stereo-matching. Zhu et al. (2020) explore the constraints from semantic segmentation to help unsupervised monocular depth estimation. Rahman & Fattah (2024) propose a depth semantics symbiosis module to achieve comprehensive mutual awareness information for boosting depth estimation. Although semantic labels are helpful, obtaining large-scale labels can be costly in many scenarios.

Compared with the semantics, low-level structure information is more accessible to compute. For example, it is easy to compute the Canny edge or Sobel edge using the famous Canny operator (Canny, 1986) and the Sobel operator (Sobel & Feldman, 1973). Pretrained deep-learning models, such as SAM (Kirillov et al., 2023), can also be used. Schenk & Fraundorfer (2017) leverage the combination of edge images and depth maps for joint camera pose estimation. In some recent work, synthetic images are used to train deep learning models, where the ground truths can be easily obtained (Zhang et al., 2019b; DeTone et al., 2018). In this work, we investigate using different low-level geometric information, such as keypoints and the edge, in the auxiliary task. The previously used edge is a special case. Our study shows that diverse low-level geometries work similarly in improving the models.

3 Method

We propose a simple yet effective geometry regularization network (GRNet) to improve the model training or fine-tuning in dense prediction tasks with limited training data. GRNet constructs a regularization term by learning from low-level keypoints or edge information via multi-task learning, as shown in Figure 1. We evaluate the proposed GRNet in generalized few-shot semantic segmentation (GFSSeg) and monocular depth estimation (MDE) tasks. As the low-level keypoints or edges used in this work are obtained via a self-supervised model or hand-crafted methods, the regularization term is self-trained and does not require any manual labels. This module is discarded in the inference stage. Therefore, the geometry regularization is a plug-and-play module and does not lead to additional computation costs at the inference stage.

In section 3.1, we first describe the auxiliary geometry regularization structure, followed by different choices of low-level geometry information in section 3.2. Our proposed primary-to-auxiliary aggregation module is depicted in section 3.3. Finally, the overall loss function is shown in section 3.4.

3.1 The Auxiliary Geometry Regularization Structure

The proposed geometry regularization module includes a low-level geometry extractor, a primary-to-auxiliary aggregation module and an auxiliary decoder, as enclosed in the dashed line in orange in Figure 1(a). The low-level geometry extractor is a non-trainable module, and there are several options, such as SIFT (Lowe, 2004), SuperPoint (DeTone et al., 2018) and Canny (Canny, 1986), which we will discuss in Section 3.2. The primary-to-auxiliary aggregation module takes the output of the primary task as one of the inputs of the auxiliary task. It considers the association between low-level structures and the primary tasks, which will be discussed in Section 3.3. The auxiliary decoder takes a simple design that includes three decoder blocks, where each includes a 1×1 convolution, a 3×3 transposed convolution and a 1×1 convolution consecutively.

3.2 Choice of Low-level Geometry Information

One important aspect of the method is the geometry information used to train the auxiliary decoder. In our study, we investigate several options, including SIFT (Lowe, 2004), SuperPoint (DeTone et al., 2018) and Canny edge (Canny, 1986). Previous studies (Song et al., 2020) often conjecture that joint edge detection provides information to smooth the output of the primary task and improves the results. Some other methods (Shao et al., 2023b) use such information to iteratively update MDE. In GRNet, we find that the keypoints and edge work similarly to improve the results in GFSS and MDE tasks. This raises a question on what is the role of edge detection in previous methods. We have conducted some experiments in our study in Section 4.2.3, and our results suggest that the post-processing iteration could be removed if we adopt the proposed GRNet to regularize the model training.

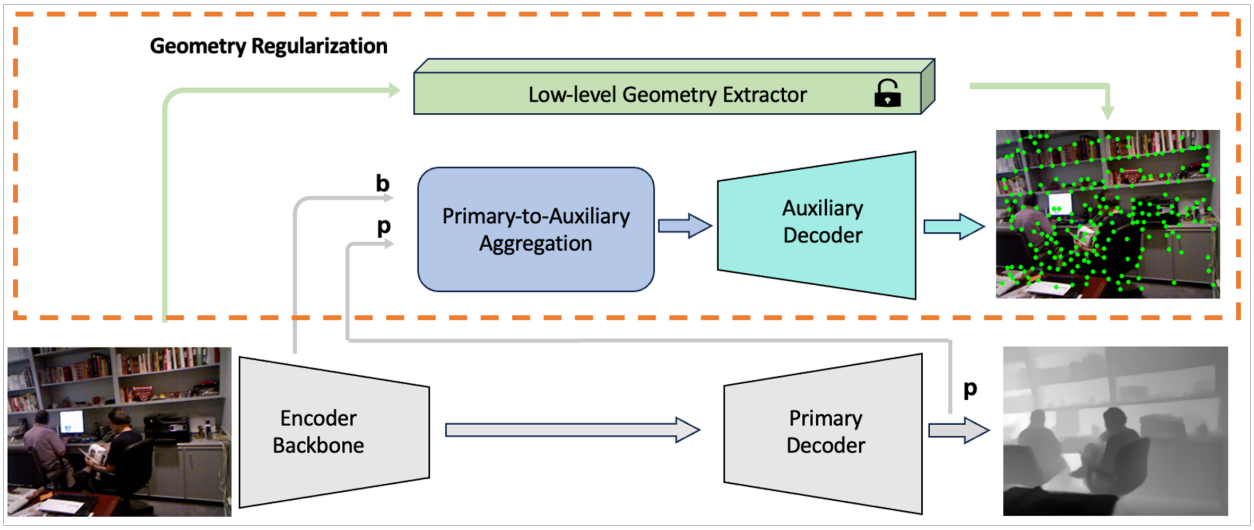

(a) The overall architecture of GRNet.

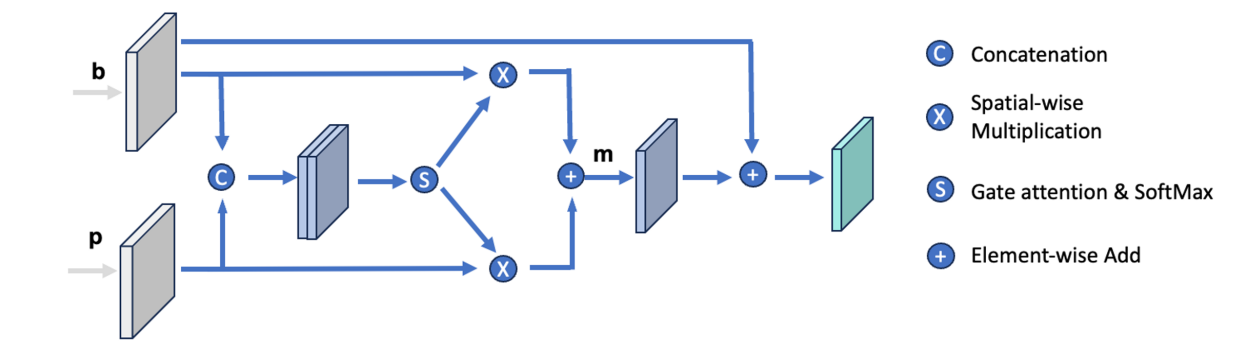

(b) The details of primary-to-auxiliary aggregation.

Figure 1: The pipeline of the proposed auxiliary self-trained geometry regularization network (GRNet). (a) GRNet consists of a low-level geometry extractor, a primary-to-auxiliary aggregation module, and an auxiliary decoder. (b) The primary-to-auxiliary aggregation module first combines two inputs, feature $\mathbf{b}$ from the encoder backbone and output $\mathbf{p}$ of the primary task, followed by gate attention and softmax to generate the correlation attention maps between primary and auxiliary tasks. The merged feature $\mathbf{m}$ results from a weighted sum of two maps multiplied by attention maps and their corresponding features. The final step includes averaging the merged feature $\mathbf{m}$ with feature $\mathbf{b}$ for auxiliary low-level geometry detection.

3.3 Primary-to-Auxiliary Aggregation

Unlike other methods that try to fuse the outputs of the low-level tasks for the primary dense prediction task, we propose a regularization at both the feature level $\mathbf{b}$ and output level $\mathbf{p}$ for the primary dense prediction task, as shown in Figure 1(a). We propose a primary-to-auxiliary (P2A) aggregation module with soft attention to achieve a one-way information flow from the primary dense prediction branch to the auxiliary low-level regularization branch. Figure 1(b) illustrates the detailed diagram of the proposed P2A aggregation module. Given feature outputs $\mathbf{b}$ and $\mathbf{p}$ extracted from the backbone and primary decoder respectively, we first concatenate them to get $\mathbf{c} = Concat(\mathbf{b}, \mathbf{p})$. Then we define two functions to map $\mathbf{c}$ via two different spatial-wise gates $G_\mathbf{b}$ and $G_\mathbf{p}$ via two 1×1 convolution. We obtain:

$$A_\mathbf{b} = G_\mathbf{b}(\mathbf{c}), A_\mathbf{p} = G_\mathbf{p}(\mathbf{c}). \tag{1}$$

The softmax function is then applied to $A_{\mathbf{b}}$ and $A_{\mathbf{p}}$ to generate $S_{\mathbf{b}}$ and $S_{\mathbf{p}}$.

$$S_{\mathbf{b}} = \frac{e^{A_{\mathbf{b}}}}{e^{A_{\mathbf{b}}} + e^{A_{\mathbf{p}}}}, S_{\mathbf{p}} = \frac{e^{A_{\mathbf{p}}}}{e^{A_{\mathbf{b}}} + e^{A_{\mathbf{p}}}}. \tag{2}$$

A merged feature $\mathbf{m}$ can be computed by a weighted sum of the map $\mathbf{b}$ and map $\mathbf{p}$:

$$\mathbf{m} = \mathbf{b} \cdot S_{\mathbf{b}} + \mathbf{p} \cdot S_{\mathbf{p}}. \tag{3}$$

We then compute $\mathbf{b}'$ as average of $\mathbf{m}$ and the feature $\mathbf{b}$ for subsequent low-level structure detection.

$$\mathbf{b}' = \frac{\mathbf{b} + \mathbf{m}}{2}. \tag{4}$$

The module is introduced to regularize the model training at the training stage and avoid converging to local minima. We do not change the network structure of existing methods. It can be discarded effortlessly after training.

3.4 Loss function

As described in section 3.3, we obtain the supervisory geometry information from the hand-crafted or pre-trained low-level extractor. We adopt the focal loss (Lin et al., 2020) to compute the loss L_{gr} for the auxiliary task, as shown in Equation (5):

$$L_{gr} = \mathcal{F}(s_{gt}, s_{est}), \tag{5}$$

where s_{gt} and s_{est} denote the pseudo low-level geometry supervision and estimated geometry from the auxiliary task, respectively. $\mathcal{F}$ denotes the function to compute focal loss.

In order to use the auxiliary task to regularize the primary task, we combine the losses of the two tasks via a weighted sum. The overall loss is computed as the weighted sum of the loss L_p from the primary dense prediction decoder and L_{gr} from GRNet, as shown in Equation (6):

$$L = L_p + \lambda \cdot L_{gr}, \tag{6}$$

where λ controls the balance of the two items and λ is set to 1 empirically in our work.

4 Experimental Results

We evaluate our methods in the generalized few-shot semantic segmentation (GFSSeg) and monocular depth estimation (MDE) tasks.

4.1 Generalized Few-shot Semantic Segmentation

4.1.1 Datasets and Evaluations

- **Datasets.** The PASCAL-5^i built on the PASCAL VOC 2012 (Everingham et al., 2010) dataset is used. It contains 12,031 images with high-quality pixel-level annotations of 20 classes, split into two sets of 10,582 and 1,449 for training and validation, respectively. Following the standard protocol in (Liu et al., 2023b; Tian et al., 2022), the 20 classes are evenly partitioned into four folds for cross-validation. Furthermore, we evaluate the capability of our method on a more challenging COCO-20^i dataset, which includes 122,218 images with 80 object classes. In between, 82,081 and 40,137 images are exploited for training and validation. Similarly, experiments on COCO-20^i are also conducted with cross-validation on four folds (20 classes per fold).

- **Evaluation Metrics.** For both datasets, once we validate the model on one fold, the classes in this fold serve as novel classes, and the classes in the other three folds plus background play the role of base classes. The Intersection over Union (IoU) per class and mean IoU (mIoU) over the base, novel, and all classes are computed. We follow the same settings as in (Tian et al., 2022; Myers-Dean et al., 2021; Liu et al., 2020; 2023a) to conduct four-fold cross-validation and calculate the average values. We also repeat each experiment with five different seeds and compute the mean values (Tian et al., 2022).

Table 1: Performance comparisons on PASCAL-5^i for GFSSeg. We report mIoU (%) over base classes (Base), novel classes (Novel), and all classes (Base + Novel = Total). All models are based on ResNet-50. † represents the use of SIFT as the constraint of our GRNet. "GRNet w A" denotes to apply GRNet on A.

Method	1-shot			5-shot			10-shot		
	Base	Novel	Total	Base	Novel	Total	Base	Novel	Total
PFENet (Tian et al., 2020)	8.32	2.67	6.97	8.83	1.89	7.18	/	/	/
PANet (Wang et al., 2019)	31.88	11.25	26.97	32.95	15.25	28.74	/	/	/
DIaM (Hajimiri et al., 2023)	70.89	35.11	61.24	70.85	55.31	68.29	/	/	/
FT (Myers-Dean et al., 2021)	66.84	18.82	55.41	72.03	46.40	65.93	73.02	52.55	68.14
FT-Triplet	66.41	19.71	55.31	71.31	50.46	66.35	72.87	57.00	69.10
CAPL (Tian et al., 2022)	65.48	18.85	54.38	66.14	22.41	55.72	69.09	27.17	59.11
GRNet w CAPL †	**69.72**	**20.18**	**57.92**	**70.51**	**28.57**	**60.53**	**72.51**	**31.01**	**62.82**
POP (Liu et al., 2023a)	**73.92**	35.51	64.77	74.78	55.87	70.28	**74.99**	58.77	71.13
GRNet w POP †	73.75	**41.12**	**66.01**	**74.80**	**57.12**	**70.89**	74.83	**59.81**	**71.52**

Table 2: Performance comparisons on COCO-20^i for GFSSeg. Models are based on ResNet-50. † represents the use of SIFT as the constraint of our GRNet.

Method	1-shot			5-shot			10-shot		
	Base	Novel	Total	Base	Novel	Total	Base	Novel	Total
DIaM	48.28	17.22	40.29	48.37	28.73	46.72	/	/	/
FT	43.42	8.94	34.90	47.18	24.72	41.63	48.18	30.03	43.70
FT-Triplet	43.64	9.23	35.14	46.61	28.84	41.36	46.61	34.49	43.27
CAPL (Tian et al., 2022)	44.61	7.05	35.46	45.24	11.05	36.80	45.51	10.82	36.95
GRNet w CAPL †	**46.26**	**9.36**	**37.16**	**46.38**	**13.30**	**38.21**	**46.38**	**14.55**	**39.63**
POP (Liu et al., 2023a)	**54.71**	15.31	44.98	**54.90**	29.97	48.75	55.01	35.05	50.08
GRNet w POP †	53.81	**19.57**	**45.36**	54.12	**31.62**	**49.27**	**55.06**	**36.18**	**50.29**

4.1.2 Implementation Details

Our GRNet is implemented on PyTorch. Following the training strategy in (Tian et al., 2022; Liu et al., 2023a), the mini-batch stochastic gradient descent with momentum 0.9 and weight decay 0.0001 is exploited to optimize the model. During the base class learning, the initial learning rate is set to 0.01, which is annealed down to zero following a "poly" policy whose power is fixed to 0.9. The batch size is 8 for both datasets, and the models are trained for 100 epochs for base class learning. For novel class updating, we update the model with a fixed learning rate of 0.01 for 500 epochs, and the batch size is set as 2 and 8 for PASCAL5^i and COCO-20^i, respectively.

4.1.3 Comparison with state-of-the-art methods

We integrate the proposed GRNet with the two latest GFSSeg methods, CAPL (Tian et al., 2022) and POP (Liu et al., 2023a), to justify its effectiveness on PASCAL-5^i and COCO-20^i datasets. We denote the method applying GRNet on baseline approach A as "GRNet w A". We choose the SIFT keypoint as the main geometry knowledge in our implementation, but the results using other low-level structures are also reported. Table 1 summarizes the mIoU performances of different settings (k-shot, $k = 1, 5, 10$) on the PASCAL-5^i dataset. Overall, the results across three different settings consistently indicate that the proposed GRNet can improve the performances of the novel classes. In particular, the mIoU performance of novel class by GRNet with the CAPL outperforms the original CAPL model by 7.1%, 27.5% and 14.1% relatively in 1-shot, 5-shot and 10-shot, respectively, while the performances for base classes are maintained or slightly improved. Similarly, the GRNet with POP outperforms the original POP by 15.8%, 2.2%, and 1.8% for novel classes in 1-shot, 5-shot, and 10-shot, respectively.

Table 1 shows that GRNet with CAPL outperforms the baseline CAPL method on base and novel classes across three different shot experiments. Meanwhile, the results of GRNet with POP are in a bit of mIoU improvement (0.02%) of base class on the 5-shot setting, even worse than that on 1-shot and 10-shot settings. We think the reason is the different training strategies between CAPL and POP. It is highlighted that the GRNet leads to a slight performance drop for base classes in POP (Liu et al., 2023a), but this does not happen in CAPL (Tian et al., 2022). This is due to the different training strategies between CAPL and POP. The former iteratively optimizes the models for the base classes and updates the novel classes in each epoch. The latter trains the models for base classes first and then updates them for the novel classes without using the data of base classes.

Table 2 details the performance comparisons of 1-shot, 5-shot, and 10-shot on COCO-20^i dataset. Similar to the experimental results on the PASCAL-5^i dataset, GRNet with POP surpasses the original POP by 27.8%, 5.5%, and 3.2% relatively on 1-shot, 5-shot, and 10-shot settings. The results again empirically verify the effectiveness of our method. Figure 2 shows three sample results for GFSSeg in PASCAL, by CAPL, POP and our methods under the 5-shot setting. As shown in the results, our methods achieve more accurate segmentation.

Next, we discuss the deeper insights revealed by the experimental results. When training data is limited or scarce in the few-shot segmentation task, the risk of over-fitting increases as the training would optimize the model for the limited training data and lead to poor generalization. Although data augmentation could help, there is still space for improvement. Our core idea is to increase the task via multi-tasking. By including the low-vision task in the few-shot semantic segmentation, we ask the network to optimize for both the primary and low-vision tasks simultaneously. Table 1 and 2 present that our proposed GRNet algorithm enhances the performance of novel classes across three different settings, demonstrating its effectiveness in reducing over-fitting and improving generalization.

4.1.4 Choice of low-level geometry extractor

Table 3: Performance comparisons of different geometry regularization on PASCAL-5^i, including SIFT, SuperPoint and Canny edge. We report mIoU (%) over base classes (Base), novel classes (Novel), and all classes (Base + Novel = Total). All models are based on ResNet-50. †, ‡ and § respectively represent the use of SIFT, SuperPoint and Canny edge as the constraints of our GRNet.

Method	1-shot			5-shot			10-shot		
	Base	Novel	Total	Base	Novel	Total	Base	Novel	Total
CAPL (Tian et al., 2022)	65.48	18.85	54.38	66.14	22.41	55.72	69.09	27.17	59.11
GRNet w CAPL †	69.72	**20.18**	57.92	**70.51**	**28.57**	60.53	**72.51**	31.01	62.82
GRNet w CAPL ‡	**70.12**	20.03	**58.19**	70.47	29.49	**60.72**	72.48	**31.25**	**62.96**
GRNet w CAPL §	69.65	20.13	57.85	70.08	29.53	60.43	72.33	30.62	62.53
POP (Liu et al., 2023a)	**73.92**	35.51	64.77	74.78	55.87	70.28	**74.99**	58.77	71.13
GRNet w POP †	73.75	**41.12**	66.01	74.70	**57.12**	**70.89**	74.83	**59.81**	**71.52**
GRNet w POP ‡	73.71	41.09	**65.98**	74.62	57.08	70.81	74.76	59.68	71.44
GRNet w POP §	73.83	40.52	65.89	**74.88**	56.99	70.65	74.98	59.67	71.34

Table 4: p values of statistic t-test between SIFT and other regularizations in 1-shot CAPL on PASCAL dataset.

SIFT vs.	Baseline	SuperPoint	Canny
p-value	0.032	0.109	0.622

To verify the effectiveness of different low-level geometry extractors, we adopt and compare the SIFT (†), SuperPoint (‡) and Canny edge (§) as low-level geometry in the GFSSeg. Table 3 shows the performance comparisons of different geometry regularizations on PASCAL-5^i. In the GRNet with CAPL, the three

different low-level geometries improve the performance of novel classes comparably. We further conduct a statistic t-test to compare SIFT regularization with SuperPoint, Canny and also the baseline without GRNet.

Table 4 shows the statistic t-test p values to validate the choice of regularizations. As we can see, there is a significant difference between the SIFT regularized model and the baseline ($p < 0.05$). The different choices of regularization terms do not lead to significant differences ($p > 0.05$), which indicates that the choice of regularization is not sensitive to the final performance.

4.1.5 Ablation Studies

We conduct ablation studies to evaluate the effectiveness of each proposed module. We use POP as a baseline. The GRNet includes two modules. The first module is a simple multi-task learning of the primary task and a low-level extraction task to detect SIFT, denoted as "Multi-task". The second module is the primary-to-auxiliary module, which considers the association between the two tasks. Table 5 summarizes the performances when the two components are used in GFSSeg. Specifically, in the case of 5-shot segmentation, the addition of the "Multi-task" component leads to an increase in the IoU metric of novel classes from 55.87 to 56.47. Furthermore, the integration of the primary-to-auxiliary module resulted in a further improvement, raising the final IoU of novel classes to 57.12. The results show that both components would improve the performances for novel classes without sacrificing much accuracy on the base classes. Multi-task learning and the primary-to-auxiliary aggregation module allow the model to generalize better.

Table 5: Ablation study for GRNet on PASCAL in the generalized few-shot segmentation.

Baseline (POP)	Multi-task	Primary-to-Auxiliary	1-shot Base/Novel/Total	5-shot Base/Novel/Total	10-shot Base/Novel/Total
✓			**73.92**/35.51/64.77	74.78/55.87/70.28	**74.99**/58.77/71.13
✓	✓		73.63/36.88/64.89	74.69/56.47/70.36	74.89/59.24/71.27
✓	✓	✓	73.75/**41.12**/**66.01**	**74.70**/**57.12**/**70.89**	74.83/**59.81**/**71.52**

Next, we investigate the impact of different λ weights on the results. Table 6 shows the performance comparisons for different hyper-parameters λ choices. The results indicate that when λ is set to 1, the proposed algorithm achieves a mIoU of 70.87 in 5-shot segmentation on the PASCAL dataset, outperforming the settings of λ at 0.1 and 0.5.

Table 6: Performance comparisons of different hyper-parameters on PASCAL-5^i with SIFT. We report mIoU (%) of all classes (Base + Novel = Total)

λ	0.1	0.5	1
GRNet w POP †	70.77	70.68	70.89

4.2 Monocular Depth Estimation

4.2.1 Datasets

We use the NYUv2 (Nathan Silberman & Fergus, 2012) and KITTI (Geiger et al., 2013) datasets to evaluate the model generalization of the proposed GRNet in MDE. NYUv2 is an indoor dataset with 120K RGB-D videos captured from 464 indoor scenes. We follow the official training/testing split to evaluate our method, where 249 scenes are used for training, and 654 images from 215 scenes are used for testing. KITTI is an outdoor dataset captured by equipment mounted on a moving vehicle, providing stereo images and corresponding 3D laser scans. The images are around 376×1241 resolution. We follow the experiment setting in (Yuan et al., 2022), which consists of 85,898 training images, 1000 validation images and 500 test images. We report the comparison results on the validation data.

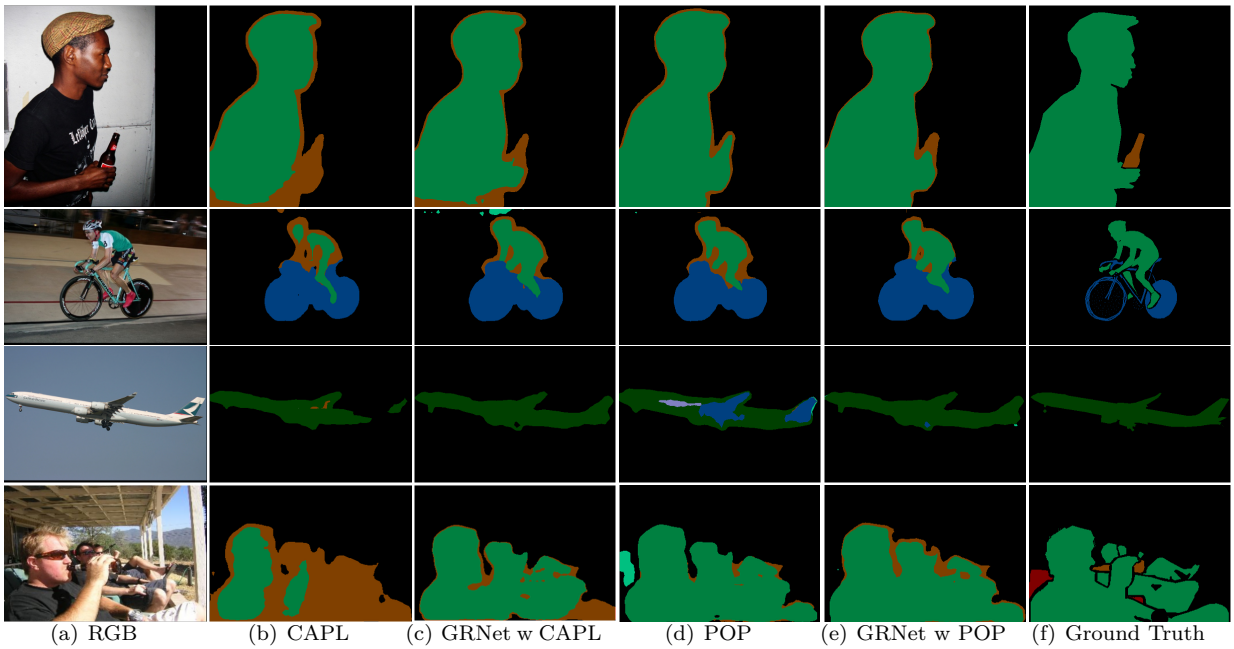

(a) RGB (b) CAPL (c) GRNet w CAPL (d) POP (e) GRNet w POP (f) Ground Truth

Figure 2: The visualization comparison of three examples from PASCAL by different methods under the 5-shot setting of GFSSeg.

4.2.2 Evaluation Metrics

Similar to previous work (Yuan et al., 2022; Shao et al., 2023b), we leverage the standard evaluation protocols in MDE, i.e., square root of the scale-invariant logarithmic error (SILog), relative absolute error (Abs Rel), relative squared error (Sq Rel), root mean squared error (RMSE), log10 error (log10), and threshold accuracy (δ <1.25). We also report the computational complexity in GFlops.

4.2.3 Comparison with state-of-the-art

Table 7: Quantitative results on NYUv2. "Abs Rel" and "RMSE" are the main ranking metrics. †, ‡ and § respectively represent the use of SIFT, SuperPoint and Canny edge as the constraints of our GRNet.

Method	Abs Rel ↓	RMSE ↓	Sq Rel↓ ↓	log10↓	δ <1.25 ↑	GFlops↓
DORN (Fu et al., 2018a)	0.115	0.509	/	0.051	0.828	/
BTS (Lee et al., 2019)	0.110	0.392	0.066	0.047	0.885	/
Adabin (Bhat et al., 2021)	0.103	0.364	/	0.044	0.903	/
P3Depth (Patil et al., 2022)	0.104	0.356	/	0.043	0.898	/
NeWCRFs (Yuan et al., 2022)	0.095	0.334	0.045	0.041	0.922	43.182
IEBins (Shao et al., 2023b)	**0.087**	**0.314**	**0.040**	**0.038**	0.936	99.068
GRNet w NeWCRFs §	0.089	0.314	0.042	0.039	0.929	43.182
GRNet w NeWCRFs †	0.088	0.314	0.041	0.039	0.929	43.182
GRNet w NeWCRFs ‡	0.088	**0.314**	0.041	**0.038**	0.929	**43.182**

Results on indoor scenes. We choose the recent NeWCRFs (Yuan et al., 2022) as our baseline and implement GRNet in NYUv2 for indoor scenes. We use three different geometries: SIFT, SuperPoint and Canny Edge. Their results are denoted by †, ‡ and § respectively. Table 7 shows that our proposed GRNet improves the depth estimation performance in the two main metrics, "Abs Rel" error and "RMSE". Specifically, the "Abs Rel" error is reduced by 7.37% relatively from 0.095 to 0.088, and the RMSE error is reduced by 5.99% relatively from 0.334 to 0.314. We also compare our method with IEBins, which proposes the Iterative Elastic Bins on top of NeWCRFs for MDE. Table 7 shows that our GRNet with NeWCRFs

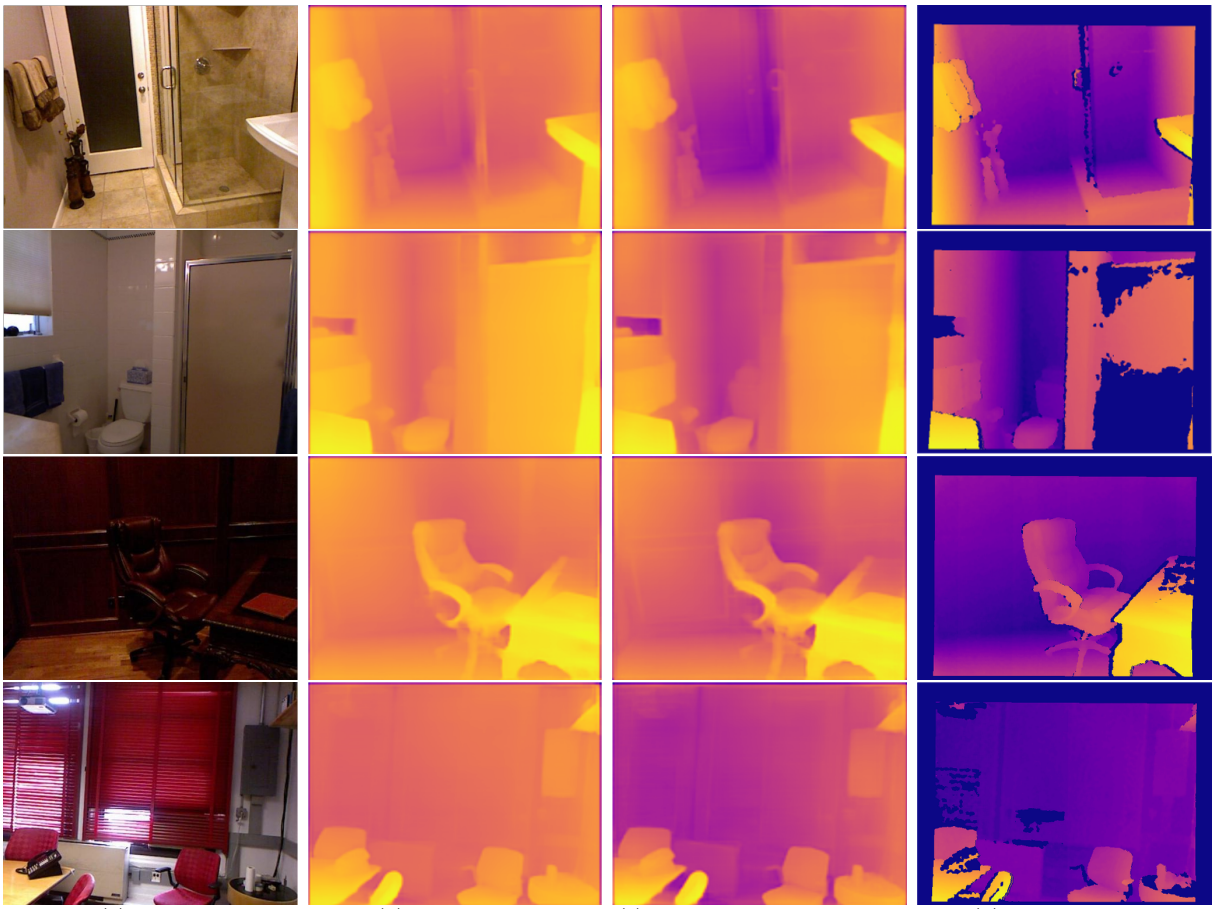

(a) RGB (b) NeWCRFs (c) GRNet with NeWCRFs (d) Ground Truth

Figure 3: Some examples of monocular depth estimation from NYUv2 by NeWCRFs (Yuan et al., 2022) and our proposed GRNet

achieves comparable performance compared with IEBins but with a 56.4% reduction in GFlops. This shows that our method could be used to replace the iterative elastic bins. Figure 3 visualizes the comparisons between NeWCRFs and our GRNet in MDE.

It is also interesting to note that different choices of geometries improve the performance of MDE comparably, similar to that in GFSSeg. Previous work (Krishna & Vandrotti, 2023) suspected that the edges provide information to smooth the output of the segmentation or depth estimation for improved performance. However, this cannot explain why the keypoints improve the performance comparable to the edge. Moreover, SuperPoint (DeTone et al., 2018) and SIFT (Lowe, 2004) differ from each other, while their improvements in the tasks here are also similar. We conjecture that the terms from either edges or points play a role of regularization instead of smoothing.

Results on outdoor scenes. We also report the results for the outdoor scenes in KITTI (Geiger et al., 2013). Table 8 summarizes the comparison with previous methods. By applying the GRNet with the recent NeWCRFs (Yuan et al., 2022) and IEBins (Shao et al., 2023b), we achieve relative reductions of the main metric SILog error by 16.6% from 8.31 to 6.93 and 9.4% from 7.58 to 6.87, respectively. The performance comparison on KITTI again proves that our GRNet could benefit the depth estimation methods for better generalization.

Table 8: Quantitative results on KITTI validation. The SILog is the main ranking metric. † represents the use of SIFT as the constraint of our GRNet.

Method	SILog ↓	Abs Rel ↓	Sq Rel ↓	RMSE ↓	δ <1.25 ↑
DORN (Fu et al., 2018a)	12.22	11.78	3.03	3.80	0.913
BTS (Lee et al., 2019)	10.67	7.51	1.59	3.37	0.938
BA-Full (Aich et al., 2021)	10.64	8.25	1.81	3.30	0.938
NeWCRFs (Yuan et al., 2022)	8.31	5.54	0.89	2.55	0.968
GRNet w NeWCRFs †	**6.93**	**4.84**	**0.76**	**2.06**	**0.979**
IEBins (Shao et al., 2023b)	7.58	5.10	0.75	2.37	0.974
GRNet w IEBins †	**6.87**	**4.70**	**0.74**	**2.01**	**0.980**

5 Conclusions

In this paper, we proposed a novel regularization term to improve the training of existing deep neural networks, especially for dense prediction tasks with limited training data, such as generalized few-shot semantic segmentation and monocular depth estimation. The proposed self-trained plug-and-play geometry regularization is discarded in the inference stage and would neither modify the network structure nor change the speed. Experimental results on different generalized few-shot semantic segmentation and monocular depth estimation methods validate the effectiveness and generalization of the proposed regularization term. A limitation of the approach is the additional time for training.

References

Shubhra Aich, Jean Marie Uwabeza Vianney, Md Amirul Islam, and Mannat Kaur Bingbing Liu. Bidirectional attention network for monocular depth estimation. In *2021 IEEE International Conference on Robotics and Automation (ICRA)*, pp. 11746–11752. IEEE, 2021.

Hangbo Bao, Li Dong, Songhao Piao, and Furu Wei. BEiT: BERT pre-training of image transformers. In *International Conference on Learning Representations*, 2022. URL `https://openreview.net/forum?id=p-BhZSz59o4`.

Shariq Farooq Bhat, Ibraheem Alhashim, and Peter Wonka. Adabins: Depth estimation using adaptive bins. In *Proceedings of the IEEE/CVF Conference on Computer Vision and Pattern Recognition*, pp. 4009–4018, 2021.

Shariq Farooq Bhat, Reiner Birkl, Diana Wofk, Peter Wonka, and Matthias Müller. Zoedepth: Zero-shot transfer by combining relative and metric depth. *arXiv preprint arXiv:2302.12288*, 2023.

John Canny. A computational approach to edge detection. *IEEE Transactions on Pattern Analysis and Machine Intelligence*, PAMI-8(6):679–698, 1986. doi: 10.1109/TPAMI.1986.4767851.

Nicolas Carion, Francisco Massa, Gabriel Synnaeve, Nicolas Usunier, Alexander Kirillov, and Sergey Zagoruyko. End-to-end object detection with transformers. In *European conference on computer vision*, pp. 213–229. Springer, 2020.

Mathilde Caron, Hugo Touvron, Ishan Misra, Hervé Jégou, Julien Mairal, Piotr Bojanowski, and Armand Joulin. Emerging properties in self-supervised vision transformers. In *Proceedings of the IEEE/CVF international conference on computer vision*, pp. 9650–9660, 2021.

Liang-Chieh Chen, George Papandreou, Iasonas Kokkinos, Kevin Murphy, and Alan L Yuille. Deeplab: Semantic image segmentation with deep convolutional nets, atrous convolution, and fully connected crfs. *IEEE transactions on pattern analysis and machine intelligence*, 40(4):834–848, 2017.

Ting Chen, Simon Kornblith, Mohammad Norouzi, and Geoffrey Hinton. A simple framework for contrastive learning of visual representations. In *International conference on machine learning*, pp. 1597–1607. PMLR, 2020.

Bowen Cheng, Ishan Misra, Alexander G Schwing, Alexander Kirillov, and Rohit Girdhar. Masked-attention mask transformer for universal image segmentation. In *Proceedings of the IEEE/CVF conference on computer vision and pattern recognition*, pp. 1290–1299, 2022.

Timothée Darcet, Maxime Oquab, Julien Mairal, and Piotr Bojanowski. Vision transformers need registers. *arXiv preprint arXiv:2309.16588*, 2023.

Jia Deng, Wei Dong, Richard Socher, Li-Jia Li, Kai Li, and Li Fei-Fei. Imagenet: A large-scale hierarchical image database. In *2009 IEEE conference on computer vision and pattern recognition*, pp. 248–255. Ieee, 2009.

Daniel DeTone, Tomasz Malisiewicz, and Andrew Rabinovich. Superpoint: Self-supervised interest point detection and description. In *Proceedings of the IEEE conference on computer vision and pattern recognition workshops*, pp. 224–236, 2018.

Alexey Dosovitskiy, Lucas Beyer, Alexander Kolesnikov, Dirk Weissenborn, Xiaohua Zhai, Thomas Unterthiner, Mostafa Dehghani, Matthias Minderer, Georg Heigold, Sylvain Gelly, et al. An image is worth 16x16 words: Transformers for image recognition at scale. In *ICLR*, 2020.

Mark Everingham, Luc Van Gool, Christopher KI Williams, John Winn, and Andrew Zisserman. The pascal visual object classes (voc) challenge. *International journal of computer vision*, 88:303–338, 2010.

Huan Fu, Mingming Gong, Chaohui Wang, Kayhan Batmanghelich, and Dacheng Tao. Deep ordinal regression network for monocular depth estimation. In *Proceedings of the IEEE conference on computer vision and pattern recognition*, pp. 2002–2011, 2018a.

Huazhu Fu, Jun Cheng, Yanwu Xu, Changqing Zhang, Damon Wing Kee Wong, Jiang Liu, and Xiaochun Cao. Disc-aware ensemble network for glaucoma screening from fundus image. *IEEE Transactions on Medical Imaging*, 37(11):2493–2501, 2018b. doi: 10.1109/TMI.2018.2837012.

Andreas Geiger, Philip Lenz, Christoph Stiller, and Raquel Urtasun. Vision meets robotics: The kitti dataset. *The International Journal of Robotics Research*, 32(11):1231–1237, 2013.

Jean-Bastien Grill, Florian Strub, Florent Altché, Corentin Tallec, Pierre Richemond, Elena Buchatskaya, Carl Doersch, Bernardo Avila Pires, Zhaohan Guo, Mohammad Gheshlaghi Azar, et al. Bootstrap your own latent-a new approach to self-supervised learning. *Advances in neural information processing systems*, 33:21271–21284, 2020.

Sina Hajimiri, Malik Boudiaf, Ismail Ben Ayed, and Jose Dolz. A strong baseline for generalized few-shot semantic segmentation. In *Proceedings of the IEEE/CVF Conference on Computer Vision and Pattern Recognition*, pp. 11269–11278, 2023.

Kaiming He, Haoqi Fan, Yuxin Wu, Saining Xie, and Ross Girshick. Momentum contrast for unsupervised visual representation learning. In *Proceedings of the IEEE/CVF conference on computer vision and pattern recognition*, pp. 9729–9738, 2020.

Kaiming He, Xinlei Chen, Saining Xie, Yanghao Li, Piotr Dollár, and Ross Girshick. Masked autoencoders are scalable vision learners. In *Proceedings of the IEEE/CVF conference on computer vision and pattern recognition*, pp. 16000–16009, 2022.

Fabian Isensee, Paul F Jaeger, Simon AA Kohl, Jens Petersen, and Klaus H Maier-Hein. nnu-net: a self-configuring method for deep learning-based biomedical image segmentation. *Nature methods*, 18(2): 203–211, 2021.

Alexander Kirillov, Eric Mintun, Nikhila Ravi, Hanzi Mao, Chloe Rolland, Laura Gustafson, Tete Xiao, Spencer Whitehead, Alexander C Berg, Wan-Yen Lo, et al. Segment anything. In *Proceedings of the IEEE/CVF International Conference on Computer Vision*, pp. 4015–4026, 2023.

Sriram Krishna and Basavaraja Shanthappa Vandrotti. Deepsmooth: Efficient and smooth depth completion. In *Proceedings of the IEEE/CVF Conference on Computer Vision and Pattern Recognition*, pp. 3357–3366, 2023.

Alina Kuznetsova, Hassan Rom, Neil Alldrin, Jasper Uijlings, Ivan Krasin, Jordi Pont-Tuset, Shahab Kamali, Stefan Popov, Matteo Malloci, Alexander Kolesnikov, Tom Duerig, and Vittorio Ferrari. The open images dataset v4: Unified image classification, object detection, and visual relationship detection at scale. *IJCV*, 2020.

Iro Laina, Christian Rupprecht, Vasileios Belagiannis, Federico Tombari, and Nassir Navab. Deeper depth prediction with fully convolutional residual networks. In *2016 Fourth international conference on 3D vision (3DV)*, pp. 239–248. IEEE, 2016.

Chunbo Lang, Gong Cheng, Binfei Tu, and Junwei Han. Learning what not to segment: A new perspective on few-shot segmentation. In *Proceedings of the IEEE/CVF conference on computer vision and pattern recognition*, pp. 8057–8067, 2022.

Jin Han Lee, Myung-Kyu Han, Dong Wook Ko, and Il Hong Suh. From big to small: Multi-scale local planar guidance for monocular depth estimation. *arXiv preprint arXiv:1907.10326*, 2019.

Feng Li, Hao Zhang, Huaizhe Xu, Shilong Liu, Lei Zhang, Lionel M Ni, and Heung-Yeung Shum. Mask dino: Towards a unified transformer-based framework for object detection and segmentation. In *Proceedings of the IEEE/CVF Conference on Computer Vision and Pattern Recognition*, pp. 3041–3050, 2023a.

Junnan Li, Dongxu Li, Silvio Savarese, and Steven Hoi. Blip-2: Bootstrapping language-image pre-training with frozen image encoders and large language models. *arXiv preprint arXiv:2301.12597*, 2023b.

Xiangtai Li, Houlong Zhao, Lei Han, Yunhai Tong, Shaohua Tan, and Kuiyuan Yang. Gated fully fusion for semantic segmentation. In *Proceedings of the AAAI conference on artificial intelligence*, volume 34, pp. 11418–11425, 2020.

Xiangtai Li, Jiangning Zhang, Yibo Yang, Guangliang Cheng, Kuiyuan Yang, Yunhai Tong, and Dacheng Tao. Sfnet: Faster and accurate semantic segmentation via semantic flow. *International Journal of Computer Vision*, 132(2):466–489, 2024.

Tsung-Yi Lin, Priya Goyal, Ross Girshick, Kaiming He, and Piotr Dollár. Focal loss for dense object detection. *IEEE Transactions on Pattern Analysis and Machine Intelligence*, 42(2):318–327, 2020. doi: 10.1109/TPAMI.2018.2858826.

Sun-Ao Liu, Yiheng Zhang, Zhaofan Qiu, Hongtao Xie, Yongdong Zhang, and Ting Yao. Learning orthogonal prototypes for generalized few-shot semantic segmentation. In *Proceedings of the IEEE/CVF Conference on Computer Vision and Pattern Recognition*, pp. 11319–11328, 2023a.

Weide Liu, Chi Zhang, Guosheng Lin, and Fayao Liu. Crnet: Cross-reference networks for few-shot segmentation. In *CVPR*, 2020.

Weide Liu, Zhonghua Wu, Yang Zhao, Yuming Fang, Chuan-Sheng Foo, Jun Cheng, and Guosheng Lin. Harmonizing base and novel classes: A class-contrastive approach for generalized few-shot segmentation. *International Journal of Computer Vision*, 2023b.

Ze Liu, Yutong Lin, Yue Cao, Han Hu, Yixuan Wei, Zheng Zhang, Stephen Lin, and Baining Guo. Swin transformer: Hierarchical vision transformer using shifted windows. In *Proceedings of the IEEE/CVF international conference on computer vision*, pp. 10012–10022, 2021.

David G. Lowe. Distinctive image features from scale-invariant keypoints. *International Journal of Computer Vision*, 2004.

Hao Lu, Wenze Liu, Hongtao Fu, and Zhiguo Cao. Fade: Fusing the assets of decoder and encoder for task-agnostic upsampling. In *European Conference on Computer Vision*, pp. 231–247. Springer, 2022.

Josh Myers-Dean, Yinan Zhao, Brian Price, Scott Cohen, and Danna Gurari. Generalized few-shot semantic segmentation: All you need is fine-tuning. *arXiv preprint arXiv:2112.10982*, 2021.

Pushmeet Kohli Nathan Silberman, Derek Hoiem and Rob Fergus. Indoor segmentation and support inference from rgbd images. In *ECCV*, 2012.

Maxime Oquab, Timothée Darcet, Théo Moutakanni, Huy Vo, Marc Szafraniec, Vasil Khalidov, Pierre Fernandez, Daniel Haziza, Francisco Massa, Alaaeldin El-Nouby, et al. Dinov2: Learning robust visual features without supervision. *arXiv preprint arXiv:2304.07193*, 2023.

Vaishakh Patil, Christos Sakaridis, Alexander Liniger, and Luc Van Gool. P3depth: Monocular depth estimation with a piecewise planarity prior. In *Proceedings of the IEEE/CVF Conference on Computer Vision and Pattern Recognition*, pp. 1610–1621, 2022.

Luigi Piccinelli, Yung-Hsu Yang, Christos Sakaridis, Mattia Segu, Siyuan Li, Luc Van Gool, and Fisher Yu. Unidepth: Universal monocular metric depth estimation. In *IEEE Conference on Computer Vision and Pattern Recognition (CVPR)*, 2024.

Md Awsafur Rahman and Shaikh Anowarul Fattah. Semi-supervised semantic depth estimation using symbiotic transformer and nearfarmix augmentation. In *Proceedings of the IEEE/CVF Winter Conference on Applications of Computer Vision*, pp. 250–259, 2024.

Pierluigi Zama Ramirez, Matteo Poggi, Fabio Tosi, S. Mattoccia, and Luigi di Stefano. Geometry meets semantics for semi-supervised monocular depth estimation. In *ACCV*, 2018.

René Ranftl, Katrin Lasinger, David Hafner, Konrad Schindler, and Vladlen Koltun. Towards robust monocular depth estimation: Mixing datasets for zero-shot cross-dataset transfer. *IEEE transactions on pattern analysis and machine intelligence*, 44(3):1623–1637, 2020.

René Ranftl, Alexey Bochkovskiy, and Vladlen Koltun. Vision transformers for dense prediction. *ICCV*, 2021a.

René Ranftl, Alexey Bochkovskiy, and Vladlen Koltun. Vision transformers for dense prediction. In *Proceedings of the IEEE/CVF international conference on computer vision*, pp. 12179–12188, 2021b.

René Ranftl, Katrin Lasinger, David Hafner, Konrad Schindler, and Vladlen Koltun. Towards robust monocular depth estimation: Mixing datasets for zero-shot cross-dataset transfer. *IEEE Transactions on Pattern Analysis and Machine Intelligence*, 44(3), 2022.

Olga Russakovsky, Jia Deng, Hao Su, Jonathan Krause, Sanjeev Satheesh, Sean Ma, Zhiheng Huang, Andrej Karpathy, Aditya Khosla, Michael Bernstein, et al. Imagenet large scale visual recognition challenge. *International journal of computer vision*, 115:211–252, 2015.

Fabian Schenk and Friedrich Fraundorfer. Combining edge images and depth maps for robust visual odometry. In *Proceedings 28th British Machine Vision Conference*, pp. 1–12, 2017.

Shuwei Shao, Zhongcai Pei, Weihai Chen, Xingming Wu, and Zhengguo Li. Nddepth: Normal-distance assisted monocular depth estimation. In *Proceedings of the IEEE/CVF International Conference on Computer Vision*, pp. 7931–7940, 2023a.

Shuwei Shao, Zhongcai Pei, Xingming Wu, Zhong Liu, Weihai Chen, and Zhengguo Li. Iebins: Iterative elastic bins for monocular depth estimation. In *Advances in Neural Information Processing Systems (NeurIPS)*, 2023b.

Nir Shlezinger, Jay Whang, Yonina C. Eldar, and Alexandros G. Dimakis. Model-based deep learning. *ArXiv*, abs/2012.08405, 2020.

Irwin Sobel and Gary Feldman. A 3x3 isotropic gradient operator for image processing. *Pattern Classification and Scene Analysis*, pp. 271–272, 1973.

Xiao Song, Xu Zhao, Liangji Fang, Hanwen Hu, and Yizhou Yu. Edgestereo: An effective multi-task learning network for stereo matching and edge detection. *International Journal of Computer Vision*, 128:910–930, 2020.

Wanjuan Su and Wenbing Tao. Efficient edge-preserving multi-view stereo network for depth estimation. In *Proceedings of the AAAI Conference on Artificial Intelligence*, volume 37, pp. 2348–2356, 2023.

Zhuotao Tian, Hengshuang Zhao, Michelle Shu, Zhicheng Yang, Ruiyu Li, and Jiaya Jia. Prior guided feature enrichment network for few-shot segmentation. *IEEE transactions on pattern analysis and machine intelligence*, 44(2):1050–1065, 2020.

Zhuotao Tian, Xin Lai, Li Jiang, Shu Liu, Michelle Shu, Hengshuang Zhao, and Jiaya Jia. Generalized few-shot semantic segmentation. In *Proceedings of the IEEE/CVF Conference on Computer Vision and Pattern Recognition*, pp. 11563–11572, 2022.

Hugo Touvron, Matthieu Cord, and Hervé Jégou. Deit iii: Revenge of the vit. In *European conference on computer vision*, pp. 516–533. Springer, 2022.

Kaixin Wang, Jun Hao Liew, Yingtian Zou, Daquan Zhou, and Jiashi Feng. Panet: Few-shot image semantic segmentation with prototype alignment. In *proceedings of the IEEE/CVF international conference on computer vision*, pp. 9197–9206, 2019.

Zhenyao Wu, Xinyi Wu, Xiaoping Zhang, Song Wang, and Lili Ju. Semantic stereo matching with pyramid cost volumes. In *2019 IEEE/CVF International Conference on Computer Vision (ICCV)*, pp. 7483–7492, 2019. doi: 10.1109/ICCV.2019.00758.

Enze Xie, Wenhai Wang, Zhiding Yu, Anima Anandkumar, Jose M Alvarez, and Ping Luo. Segformer: Simple and efficient design for semantic segmentation with transformers. *Advances in neural information processing systems*, 34:12077–12090, 2021.

Gangwei Xu, Xianqi Wang, Xiaohuan Ding, and Xin Yang. Iterative geometry encoding volume for stereo matching. In *Proceedings of the IEEE/CVF Conference on Computer Vision and Pattern Recognition*, pp. 21919–21928, 2023a.

Zunnan Xu, Zhihong Chen, Yong Zhang, Yibing Song, Xiang Wan, and Guanbin Li. Bridging vision and language encoders: Parameter-efficient tuning for referring image segmentation. In *Proceedings of the IEEE/CVF International Conference on Computer Vision*, pp. 17503–17512, 2023b.

Lihe Yang, Bingyi Kang, Zilong Huang, Xiaogang Xu, Jiashi Feng, and Hengshuang Zhao. Depth anything: Unleashing the power of large-scale unlabeled data. *arXiv preprint arXiv:2401.10891*, 2024.

Changqian Yu, Jingbo Wang, Chao Peng, Changxin Gao, Gang Yu, and Nong Sang. Learning a discriminative feature network for semantic segmentation. In *Proceedings of the IEEE conference on computer vision and pattern recognition*, pp. 1857–1866, 2018.

Weihao Yuan, Xiaodong Gu, Zuozhuo Dai, Siyu Zhu, and Ping Tan. Neural window fully-connected crfs for monocular depth estimation. pp. 3916–3925, 2022.

Junming Zhang, Katherine A. Skinner, Ram Vasudevan, and Matthew Johnson-Roberson. Dispsegnet: Leveraging semantics for end-to-end learning of disparity estimation from stereo imagery. *IEEE Robotics and Automation Letters*, 4:1162–1169, 2019a.

Tianyang Zhang, Huazhu Fu, Yitian Zhao, Jun Cheng, Mengjie Guo, Zaiwang Gu, Bing Yang, Yuting Xiao, Shenghua Gao, and Jiang Liu. Skrgan: Sketching-rendering unconditional generative adversarial networks for medical image synthesis. In Dinggang Shen, Tianming Liu, Terry M. Peters, Lawrence H. Staib, Caroline Essert, Sean Zhou, Pew-Thian Yap, and Ali Khan (eds.), *Medical Image Computing and Computer Assisted Intervention – MICCAI 2019*, pp. 777–785, Cham, 2019b. Springer International Publishing.

Hengshuang Zhao, Jianping Shi, Xiaojuan Qi, Xiaogang Wang, and Jiaya Jia. Pyramid scene parsing network. In *Proceedings of the IEEE conference on computer vision and pattern recognition*, pp. 2881–2890, 2017.

Bolei Zhou, Hang Zhao, Xavier Puig, Sanja Fidler, Adela Barriuso, and Antonio Torralba. Scene parsing through ade20k dataset. In *Proceedings of the IEEE conference on computer vision and pattern recognition*, pp. 633–641, 2017.

Shengjie Zhu, Garrick Brazil, and Xiaoming Liu. The edge of depth: Explicit constraints between segmentation and depth. In *Proceedings of the IEEE/CVF conference on computer vision and pattern recognition*, pp. 13116–13125, 2020.